Effect of Pressurization on Airplane Fuselage Drag

DEZSO GYORGYFALVY*
The Boeing Company, Renton, Wash.

Cabin pressurization in transport airplanes tends to form bulges in the fuselage skin between the frames and stringers, and the resulting wavy surface is liable to produce a higher aerodynamic drag. A flight test study has been made to determine the effect of pressurization on the fuselage drag of a Boeing 720 jetliner. The study is based on boundary-layer measurements, made by pitot-static rakes at several points of the fuselage in both pressurized and unpressurized conditions. The effect of pressurization is manifested in an increased boundary-layer momentum thickness. The analysis indicates that the drag coefficient of the fuselage is increased by approximately 5% as a result of the pressurization. It appears, however, that only a lesser part of this drag increment is caused by the skin bulging, and the greater part is caused by leakage of the pressurized air or exhaust-air associated with the pressurization system.

Nomenclature

c_f = local skin-friction coefficient,$_0/q_\infty$
L = length of fuselage, ft
p = static pressure, psf
p_t = total pressure, psf
q = dynamic pressure, $(\rho/2)U^2$, psf
q_c = impact pressure, $p_t - p$, psf
U = velocity, fps
U_τ = "friction velocity," $(\tau_0/\rho_0)^{1/2}$, fps
T = static temperature, °K
x = coordinate parallel to the centerline of fuselage, ft
y = coordinate perpendicular to the surface, ft
z = coordinate perpendicular to x and y, ft
δ^* = boundary-layer displacement thickness, ft
θ = boundary-layer momentum thickness, ft
ν = kinematic viscosity, ft/sec^2
ρ = air density, lb sec^2/ft^4
τ = shearing stress, psf

Subscripts

∞ = freestream value
1 = local value at the boundary-layer edge
y = local value within the boundary layer or wake
0 = value at the surface

Introduction

In today's aircraft industry it is not unusual that a new airplane is marketed and sold in quantity even before the prototype has made its first flight. Performance guarantees play a key role in such marketing and this, of course, requires a high degree of accuracy in the airplane's aerodynamic design, especially in the prediction of the drag. A thorough knowledge of the sources of drag is therefore of great importance for the designer to accomplish his job.

Skin friction is a major source of drag in modern subsonic airplanes. It depends primarily on the Reynolds number and the type of the boundary layer, but it is also influenced by compressibility, pressure gradient, and surface roughness. The drag prediction accuracy greatly depends upon the proper appraisal of these second-order effects. It is especially difficult to estimate the drag increment caused by roughness or surface irregularities, which include rivet heads, seams, joints, gaps, holes, scratches, paint-grains, and surface waves, etc. Therefore, a great deal of research work has been recently directed toward learning more about the effects of surface irregularities.

One interesting topic along this line is the surface waviness that is manifested in a very distinct form on the fuselage of large transport airplanes under pressurization. As shown in Fig. 1, the cabin overpressure deforms the skin between the frames and stringers, thus developing a series of bulges in the fuselage surface. Following this observation, the question has been raised: to what extent does the bulging of the fuselage skin caused by the pressurization affect the drag?

Theoretical considerations indicate that the growth of the boundary layer is greater, therefore the drag is higher, for a wavy surface than for a smooth surface. The drag increment caused by surface waviness can be estimated on the basis of Schlichting's approximate formula (Ref. 1, p. 623). For fully turbulent flow,

$$C_D = C_F\left[\int_0^1 \left(\frac{U_1}{U_\infty}\right)^{3.5} d\left(\frac{x}{\ell}\right)\right]^{0.8} \tag{1}$$

where C_D is the drag coefficient of the wavy surface, C_F is the corresponding smooth flat-plate skin-friction coefficient, U_1/U_∞ is the ratio of the local velocity to the freestream velocity, and ℓ is the chord length.

Considering a surface perturbed by sinusoidal waves, one can write the local velocity as $U_1 = U_\infty + u$. For the perturbation velocity component u, Ref. 2 gives

$$u = (2\pi/m)(\epsilon/\lambda)U_\infty \sin[2\pi(x/\lambda)] \tag{2}$$

where ϵ is the wave amplitude, λ is the wavelength, and m is a factor depending on the Mach number.

Thus Eq. (1) can be written as

$$C_D = C_F\left[\int_0^1 \left(1 + \frac{u}{U_\infty}\right)^{3.5} d\left(\frac{x}{\ell}\right)\right]^{0.8} \tag{3}$$

Expanding the integrand in series and neglecting the higher than second-order terms, we obtain

$$C_D = C_F\left\{\int_0^1 \left[1 + 3.5\frac{u}{U_\infty} + 4.37\left(\frac{u}{U_\infty}\right)^2 + \ldots\right] \times d\left(\frac{x}{\ell}\right)\right\}^{0.8} \tag{4}$$

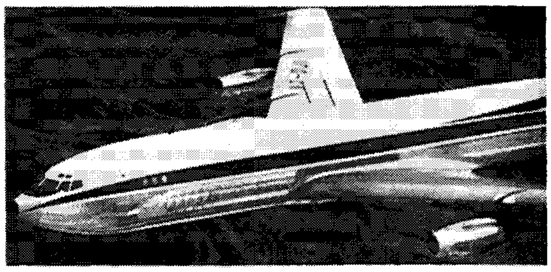

Fig. 1 **Bulging of the fuselage skin because of pressurization.**

Received January 15, 1965; revision received May 12, 1965.

* Aerodynamics Engineer, Aerodynamics Research Group, Airplane Division.

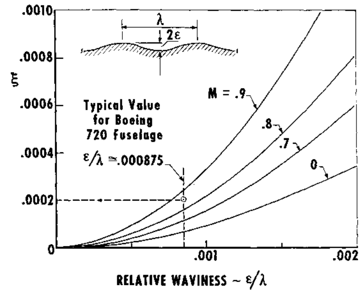

Fig. 2 The factor ξ, expressing the drag increment per wavelength.

Putting the expression of u, given by Eq. (2), into Eq. (4) and performing the integration we finally get

$$C_D = C_F[1 + 2.185n(2\pi/m)^2(\epsilon/\lambda)^2]^{0.8} = C_F(1 + n\xi)^{0.8} \quad (5)$$

where n is the number of waves. The factor ξ is plotted in Fig. 2 as a function of the relative waviness ϵ/λ for various freestream Mach numbers.

Measurements were made on a Boeing 720 fuselage during its routine pressurization test on the assembly line to determine the actual size of the surface bulges. At a typical location, where the thickness of the skin is 0.05 in. and the spacing between the frames is $\lambda = 20$ in., the bulge height was $2\epsilon = 0.035$ in. at the maximum permitted cabin overpressure of $\Delta p = 8.6$ psi. This corresponds to a relative waviness of $\epsilon/\lambda = 0.000875$, for which Fig. 2 gives $\xi \cong 0.0002$ at $M = 0.86$. If the number of waves along the fuselage is taken as $n = 50$, then Eq. (5) gives a drag increment of

$$C_{D_{\text{wavy}}}/C_{D_{\text{smooth}}} = (1 + 0.01)^{0.8} = 0.8\%$$

This simple calculation gives some idea of the drag increment caused by surface waviness, but it is probably insufficient to describe the conditions applicable to a fuselage. Even more sophisticated theoretical treatments seem to be of doubtful value because of the nonuniformity of the bulging and the complexity of the flow around the fuselage, as well as the difficulties of taking into account the effect of leakage or certain air outflows associated with the pressurization system. An experimental investigation, however, could be expected to produce more realistic results. Thus, a flight test study was conducted by the Aerodynamic Research Unit of the Boeing Company's Airplane Division in order to determine the effect of pressurization on airplane fuselage drag.

It is evident that any drag increment caused by the pressurization would be reflected on the characteristics of the fuselage boundary layer. The investigation, therefore, could be based on boundary-layer measurements taken at selected points of a fuselage in both pressurized and unpressurized conditions. At the same time, such a study could be expected to produce valuable data on the fuselage boundary-layer flow of current jet transports, data that have not previously been available.

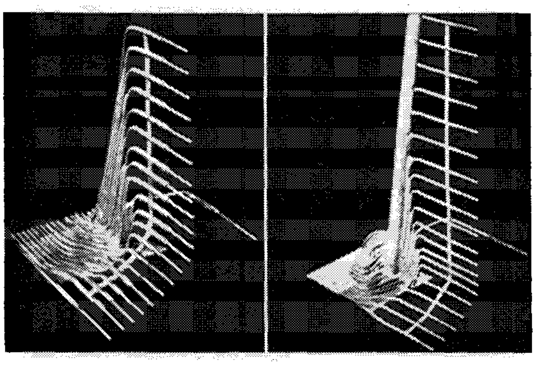

a) 6 in. high b) 12 in. high

Fig. 3 Boundary-layer rakes used.

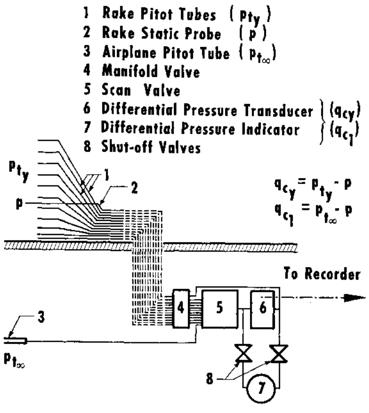

Fig. 4 Rake instrumentation scheme.

Apparatus and Test Conditions

The boundary-layer measurements were made by pitot-static rakes that incorporated 20 total pressure tubes, located at various heights above the surface, and one single static pressure probe. The static pressure is constant within the boundary layer; therefore, the location of the static probe is not critical as long as it is not very close to the surface or to the total pressure probes. Two rake sizes have been used: 6 and 12 in. high. Figure 3 shows the configuration of the rakes.

The rake instrumentation is demonstrated in Fig. 4. The rake pressures are first led to a manifold valve, which, in open position, enables the pressurized cabin air to blow through the tubing to remove water or dust clogs. The same valve, when closed, admits the rake pressures to a differential pressure transducer, which provides the electrical signal for the recording oscillograph. A scanning valve is incorporated between the manifold valve and the transducer to read the rake total pressures one by one. In addition, a differential pressure gage is connected parallel to the transducer to allow visual indication or manual recording of the rake pressures. The freestream total pressure taken from the pitot-tube of the airplane is also read into the data in order to obtain an independent reading of the local impact pressure at the outer edge of the boundary layer ($q_{c_1} = p_{t_\infty} - p$). This is especially important when the boundary-layer thickness is greater than the height of the rake; consequently, the outermost rake probe reads a lower impact pressure than q_{c_1}.

The tests were conducted on a Boeing 720 production airplane. Figure 5 shows the selected test stations. These were located on the left side of the fuselage, and it was assumed that the conditions on the other side would be identical because of symmetry. To insure an undisturbed flow upstream of each test station, the measurements were taken in three separate flights, one for each test section. Although it would have been desirable to make a more detailed survey, costs and limited airplane availability fixed the number of test stations.

The measurements were taken in a straight level flight at a nominal Mach number of $M_\infty = 0.86$ and an altitude of 25,000 ft, which represents a typical high-speed cruise condition. The data first were taken in the pressurized condition during which time the maximum permitted cabin overpressure $\Delta p = 8.6$ psi was maintained. After this the cabin was depressurized, and the data recording was repeated.

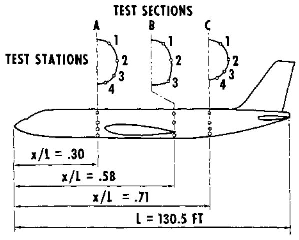

Fig. 5 Location of the test stations.

Boundary-Layer Velocity Profiles

The boundary-layer velocity profiles $U/U_1 = f(y)$ were determined from the rake surveys in the following way. First, the recorded impact pressures $q_{c_y} = p_{t_y} - p$ were corrected to compensate for small airspeed variations during the survey that are more or less inevitable in flight testing. The variations of the airspeed during the time interval required to scan the rake probes will, of course, be reflected on the boundary-layer impact pressure readings, causing distortions in the recorded profile. The corrected value of q_{c_y} was obtained by

$$q_{c_y} = q_{c_y}{}^*(\bar{V}_I/V_I{}^*)^2 \tag{6}$$

where $q_{c_y}{}^*$ and $V_I{}^*$ are the instantaneous readings of the boundary-layer impact pressures and the airplane's indicated airspeed, respectively, and $\bar{V}_I$ is the mean value of $V_I{}^*$ during the scanning.

The local static pressure p, sensed by the rake static probe, is defined as

$$p = p_{t_\infty} - q_{c_1} = p_I + q_{c_I} - q_{c_1} \tag{7}$$

where p_I and q_{c_I} are the static and impact pressures indicated by the airplane's pitot-static system (pressure altitude and indicated airspeed readings), and q_{c_1} is the impact pressure at the edge of the boundary layer ($q_{c_1} = p_{t_\infty} - p$). The local static pressure also varied during the survey because of fluctuations in airspeed or altitude; the appropriate corrections, however, proved to be negligible.

From the corrected values of q_{c_y} and p, the local Mach numbers within the boundary layer were calculated by

$$M_y = \left([2/(\gamma - 1)]\{[(q_{c_y}/p) + 1]^{(\gamma-1)/\gamma} - 1\}\right)^{1/2} \tag{8a}$$

and, likewise, the local Mach number at the edge of the boundary layer by

$$M_1 = \left([2/(\gamma - 1)]\{[(q_{c_1}/p) + 1]^{(\gamma-1)/\gamma} - 1\}\right)^{1/2} \tag{8b}$$

where $\gamma = 1.4$ for air. Hence, the velocity ratio was obtained as

$$U/U_1 = (M_y/M_1)(T_y/T_1)^{1/2} \tag{9}$$

where T_y/T_1 is the temperature ratio defined by

$$T_y/T_1 = \{1 + [(\gamma - 1)/2]M_1{}^2\}/\{1 + [(\gamma - 1)/2]M_y{}^2\} \tag{10}$$

The resulting boundary-layer velocity profiles are plotted in Fig. 6–8. At certain locations (A-1, B-3, and C-3) the difference between the profiles in pressurized and unpressurized conditions is clearly noticeable: the boundary layer is thicker, and the velocity defect within the boundary layer is considerably greater in the pressurized condition. For the majority of the test stations, however, the effect of pressurization on the profiles appears to be quite small, and in some cases it is indiscernible because of experimental scatter. Nevertheless, detailed analysis shows that, even here, there are consistent differences between the profiles, the displacement thickness and the momentum thickness always being somewhat greater in the pressurized condition.

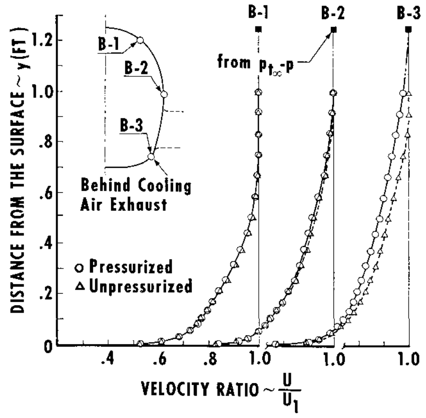

Fig. 7 Boundary-layer velocity profiles at Section B ($x/L = 0.58$).

The marked thickening of the boundary layer at the station A-1 probably results from leakage of the pressurized air through seals of the cockpit windows or the front cabin door and not from the skin bulging. The skin is relatively thick here, thus the bulging must be small, and the number of bulges ahead of this station does not seem to be sufficient to warrant such a drastic change in the boundary layer.

The profiles recorded at the station A-3 look abnormal: the velocity fails to increase with increasing distance from the surface in the usual manner, and a considerable discrepancy exists between the velocity recorded by the outermost rake probe and the velocity at the boundary-layer edge derived from $q_{c_1} = p_{t_\infty} - p$. This suggests that the boundary-layer thickness is greater here than the height of the rake. Thus, the outer region of the profiles is estimated, so that all further data pertaining to the station A-3 should be regarded only as approximate. The effect of the pressurization is obscured here by the scatter of the test points. The unusual shape of the profiles is probably a consequence of strong three-dimensional effects, such as vortex formation, which may result from wing interaction with the basic fuselage flow.

In the case of test section B (Fig. 7), the effect of pressurization is most prominent at the station B-3. This station, however, is located directly downstream of an opening through which air-conditioner cooling-air is exhausted when the pressurization system is in operation. Dumping of low-energy air into the boundary layer causes this intense thickening.

In the case of section C (Fig. 8), the effect of pressurization is apparent at all of the test stations except one. There is no difference in the profiles at the top (C-1) where the skin is thick, hence the bulging is small; but going downwards along the side, the deviation between the profiles becomes more and more noticeable. At the bottom station (C-4), however,

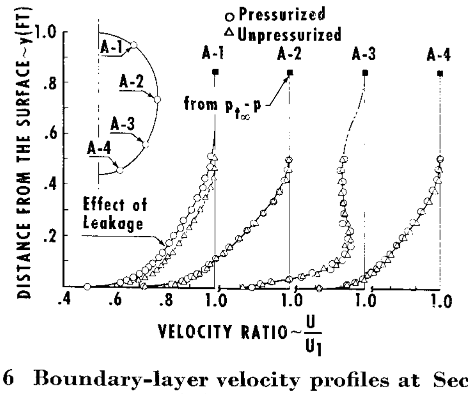

Fig. 6 Boundary-layer velocity profiles at Section A ($x/L = 0.30$).

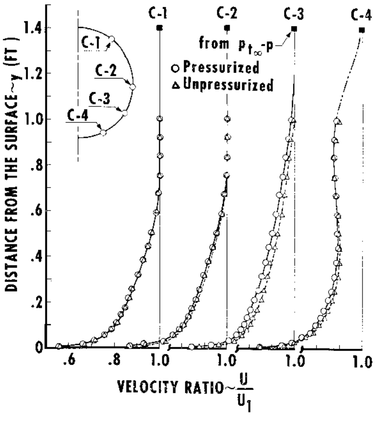

Fig. 8 Boundary-layer velocity profiles at Section C ($x/L = 0.71$)

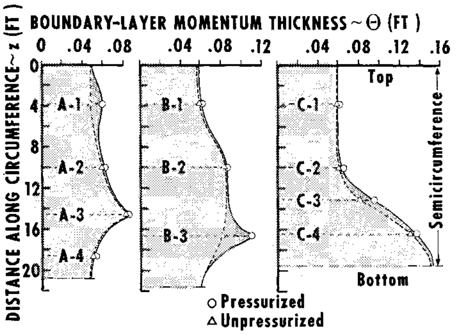

Fig. 9 Variation of the boundary-layer momentum thickness along the test sections.

the profiles again show an unusual shape with similar features as described in connection with the station A-3. There is probably a vortex shedding from the bottom of the fuselage as a result of wing interference. Because of the abnormal flow conditions, the effect of the pressurization is obscured throughout the upper region of the profile. This makes the extrapolation above $y = 1.0$ ft somewhat arbitrary. It is not critical, however, since the outer portion of the profile contributes little to the momentum loss upon which our drag estimation is based.

From the velocity profiles presented, it is evident that the pressurization has adverse effects on the fuselage boundary layer which lead to an increased drag. It is also clear that the adverse effects stem not only from the skin bulging, but also from leakage and air outflows associated with the pressurization system.

As a further step of the analysis, the following quantities are calculated from the velocity profiles (Ref. 1, p. 357):

Displacement Thickness

$$\delta^* = \int_0^\delta \left(1 - \frac{\rho_y}{\rho_1}\frac{U}{U_1}\right) dy \tag{11}$$

Momentum Thickness

$$\theta = \int_0^\delta \frac{\rho_y}{\rho_1}\frac{U}{U_1}\left(1 - \frac{U}{U_1}\right) dy \tag{12}$$

Shape Parameter

$$H = \delta^*/\theta \tag{13}$$

where $\rho_y/\rho_1 = T_1/T_y$. The results are given in Table 1.

Boundary-Layer Momentum Thickness

For drag calculation purposes the momentum thickness is the most important boundary-layer property. It can be seen from Table 1 that the momentum thickness is, almost without exception, greater in the pressurized condition than in the unpressurized condition. The increment, however, is quite small (between 1 and 3%) in most cases, and only at the stations A-1, B-3, and C-3 are larger differences noticed. Figure 9 illustrates these data depicting the variation of the momentum thickness along the semicircumference for the three test sections. The effect of the pressurization is manifested in two ways: 1) a small increment in θ more or less evenly distributed along the surface and growing in magnitude toward the rear of the fuselage and 2) marked increments in θ at certain locations. The former is probably a result of the surface bulging, whereas the latter is caused by prominent local effects. At sections A and B these local effects, namely, leakage and air exhaust, are predominant and seem to overshadow the effect of the surface bulging. At section C, however, there are no distinct local effects, and the increment in θ appears to be distributed over the entire section except the top. Evidently, this is the representative case depicting the over-all effect of the pressurization. The increment in θ, of course, stems not only from the skin bulging but also from local effects encountered upstream which become absorbed in it. Thus, it is not possible to delineate, from the present measurements, the drag effect of the skin bulging alone; the drag increment we can derive includes the effects of leakage and outflows also.

Some questions may be raised as to the validity of the data obtained at the stations A-3 and C-4, where abnormal boundary-layer profiles have been detected. It is to be noted, however, that when the local conditions are reduced to far downstream conditions in a later phase of the analysis, the relative importance of test section A becomes greatly reduced, and the reading of station A-3 is no longer as dominant as it appears in Fig. 9. On the other hand, it is unlikely that the extrapolation of the profiles in the case of A-3 and C-4 would introduce any significant error in θ, since the outer portion of the profile has little effect on the momentum thickness.

It is interesting to note here that the streamwise growth of the momentum thickness is very small along the top of the fuselage, although it is rather intense along the side and especially under the bottom. Apparently, this is a result of secondary flows induced by the wing circulation, which tends to divert the streamlines downward behind the wing. The boundary layer that originally develops at the top of the fuselage is later washed down to the sides.

Pressure Distribution around the Fuselage

The pressure distribution plays an important role in the boundary-layer development; therefore, a closer look at the local pressures around the fuselage will be helpful to better understand and interpret the test results. The local pressure coefficients $c_p = (p - p_\infty)/q_\infty$, as determined by the present experiment, are plotted in Fig. 10. Also shown are curves depicting the variation of c_p along the top, the side, and the bottom of the fuselage. These curves are based on wind-tunnel

Table 1 Tabulation of boundary-layer displacement thickness momentum thickness, and shape parameter

Test station	A				B			C			
	1	2	3[a]	4	1	2	3	1	2	3	4[a]
δ^*, in.											
Pressurized	1.006	1.160	1.46	0.890	1.150	1.588	2.031	1.061	1.146	1.768	2.478
Unpressurized	0.733	1.127	1.46	0.875	1.128	1.573	1.513	1.061	1.127	1.476	2.405
θ, in.											
Pressurized	0.722	0.741	1.02	0.618	0.727	1.026	1.318	0.704	0.752	1.133	1.663
Unpressurized	0.569	0.723	1.02	0.606	0.707	1.015	0.979	1.706	0.740	0.970	1.594
H											
Pressurized	1.390	1.560	1.43	1.440	1.580	1.550	1.540	1.510	1.52	1.560	1.510
Unpressurized	1.290	1.560	1.43	1.440	1.590	1.550	1.540	1.500	1.52	1.520	1.510

[a] Approximate values caused by nonsteady flow conditions.

test results obtained with the Boeing 367-80 prototype model.

A noteworthy feature of the flowfield around the fuselage is that favorable pressure gradients and adverse pressure gradients alternate. This results mainly from the interaction of the wing. The flow deceleration in the region of $0.15 < x/L < 0.30$ and the subsequent acceleration at $0.30 < x/L < 0.45$ is especially prominent along the side of the fuselage. The strong transverse pressure gradients in the vicinity of test section A cause cross-flow components pointing from the side to the top and to the bottom which, in turn, tend to produce a vortex flow. This was evidenced at station A-3 by the unusual boundary-layer profile recorded there. Figure 10 also shows that in the vicinity of $x/L = 0.15$ and $x/L = 0.45$ the local velocities at the side and the top of the fuselage are approaching the sonic limit. These areas, therefore, are especially critical for surface disturbances that may cause local shock wavelets.

Estimation of the Fuselage Drag and the Drag Increment Caused by Pressurization

Thus far it has been shown that the pressurization results in a certain increment in the boundary-layer momentum thickness, which is quite significant at certain locations and rather small at others. To answer the basic question of this investigation we will express this increment of θ in terms of drag coefficient. Although the experimental data pertain to only three intermediate sections along the fuselage, it is still possible to extrapolate the results to the entire fuselage and make a reasonably good estimate of the fuselage drag and the drag increment caused by pressurization.

The drag of a three-dimensional body can be calculated from the momentum equation by taking a section of the wake far downstream, where the local static pressure is equal to the freestream static pressure[3]:

$$D = 2\pi \int_0^\infty \rho U(U_\infty - U)y\,dy \tag{14}$$

where U is the local velocity within the wake, and y is the distance perpendicular to the centerline of the wake. With the preceding definition of D, the drag coefficient can be expressed as

$$C_D = \frac{2D}{\rho_\infty U_\infty{}^2 A} = \frac{4\pi}{A}\int_0^\infty \frac{\rho}{\rho_\infty}\frac{U}{U_\infty}\left(1 - \frac{U}{U_\infty}\right) y\,dy \tag{15}$$

where A is the wetted area of the body. Using the notation

$$\varkappa_\infty = 2\pi \int_0^\infty \frac{\rho}{\rho_\infty}\frac{U}{U_\infty}\left(1 - \frac{U}{U_\infty}\right) y\,dy \tag{16}$$

which is called the momentum area of the wake far downstream, the drag coefficient becomes simply

$$C_D = 2\varkappa_\infty/A \tag{17}$$

This is the three-dimensional equivalent of the well-known formula for the drag coefficient of airfoils or two-dimensional bodies:

$$C_D = 2\theta_\infty/\ell \tag{18}$$

where θ_∞ is the momentum thickness far downstream, and ℓ is the chord length.

Squire and Young[4] have shown that it is not necessary to know the far downstream value of θ in order to calculate the drag coefficient as long as the properties of the boundary layer at the trailing edge are known. Thus, the local value of θ can be reduced to the far downstream conditions by

$$\theta_\infty = \theta_\ell(U_1/U_\infty)_\ell{}^{(H_\ell+5)/2} \tag{19}$$

or by analogy

$$\varkappa_\infty = \varkappa_L(U_1/U_\infty)_L{}^{(H_L+5)/2} \tag{20}$$

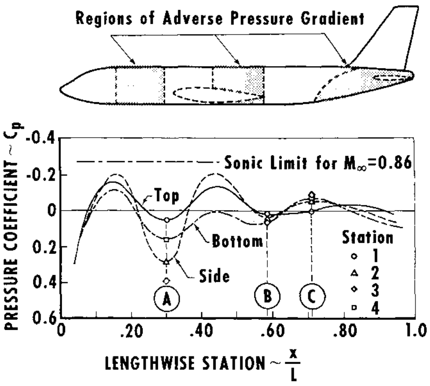

Fig. 10 Pressure distribution along the fuselage.

where the subscripts ℓ and L denote conditions at the trailing edge and tail point, respectively.

In the present case, we do not have data relevant to the tail point but for three intermediate sections along the fuselage. Nevertheless, we may assume that Squire and Young's relation is applicable to other points along the body and not only to the trailing edge. Therefore, we can take the momentum area for the three test sections and reduce it to far downstream conditions according to the Squire and Young rule, then extrapolate the data to the entire fuselage length to obtain $\varkappa_\infty$ and C_D.

Since not only θ but also U_1 and H vary along the circumference, the expression for the reduced momentum area at a given section becomes

$$\varkappa_{\infty x} = 2\int_0^{C/2} \theta_x \left(\frac{U_1}{U_\infty}\right)_x^{(H_x+5)/2} dz \tag{21}$$

It is to be noted here that the reduction term $(U_1/U_\infty)^{(H+5)/2}$ becomes more and more powerful as the velocity ratio deviates from unity. This effect is especially prominent at test station A-3 where the flow is markedly decelerated as a result of the wing interaction ($U_1/U_\infty \cong 0.76$). Although θ itself is much higher at this point than at any other point of section A (see Fig. 9), the reduced value of θ becomes only about 40% of the measured value. Thus, the uncertainties rising from the abnormal behavior of the boundary layer at station A-3 become less critical.

A plot of the reduced momentum area as a function of the fuselage wetted area is shown in Fig. 11. An increment in $\varkappa_{\infty x}$ in the pressurized condition is clearly noticeable for all three test sections. The curves passing through the experimental data are extrapolated to $A = 4200$ ft^2, the entire fuselage wetted area. Thus the following values are obtained for the total reduced momentum area: $\varkappa_\infty = 4.00$ ft^2(unpressurized) and $\varkappa_\infty = 4.20$ ft^2 pressurized. Accordingly, the drag coefficient of the fuselage $C_D = 2\varkappa_\infty/A$ becomes 0.0019 (unpressurized) and 0.0020 (pressurized). Hence

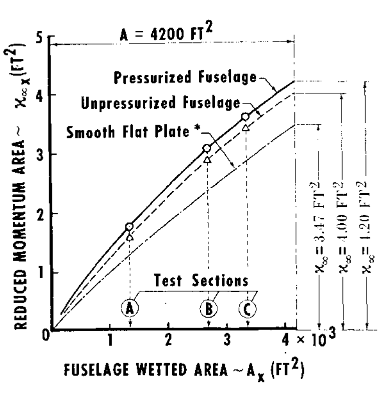

Fig. 11 Growth of the reduced momentum area.

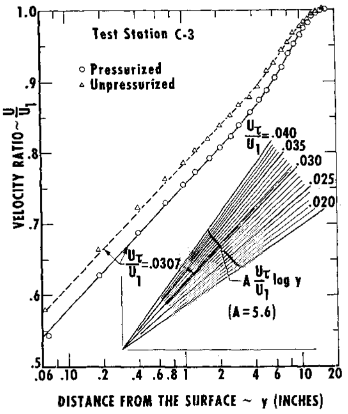

Fig. 12 Determination of the local skin-friction coefficient by the "wall-law-slope" method.

the increment in the drag coefficient caused by the pressurization is

$$\Delta C_D = 0.0001$$

which amounts to

$$\Delta C_D/C_{D_{upr}} = 5.26\%$$

The theoretical curve for a fully turbulent smooth flat plate of equal wetted area is also included in Fig. 11 for comparison. This represents the basic turbulent skin friction for $R_x = 3.0 \times 10^6$/ft and $M_\infty = 0.86$. The experimental data, of course, fall above this curve, and the difference represents the combined effect of supervelocities, surface roughness, and pressure drag.

From the designer's point of view, it is interesting to note that the increase of the fuselage drag coefficient over that of the flat plate is 15.1% in the unpressurized condition and 21.2% in the pressurized condition. These figures check quite well with the results of current drag estimation techniques.

Local Skin-Friction Coefficients

It is interesting to examine the effect of pressurization on the local skin-friction coefficient. The local skin-friction coefficient $c_f = (2\tau_0/\rho_1 U_1^2)$ can be evaluated from boundary-layer velocity profiles using the unique relation between the local velocity U and the shear stress at the wall τ_0, which is expressed by the "law of the wall":

$$U/U_\tau = A \log(yU_\tau/\nu) + B \tag{22}$$

where A and B are constants and $U_\tau = (\tau_0/\rho_0)^{1/2}$ is called the "friction velocity." The velocity profile, plotted in the terms of the law of the wall, thus appears as a straight line with a slope determined by A and an intercept determined by B. These constants have been evaluated from experimental data; therefore, slightly different values are suggested by various authors. For example, $A = 5.6$ is a widely accepted value; B is a function of the surface roughness: $B = 4.9$ has been suggested for smooth surfaces, and with increasing roughness B is decreasing.

Several methods have been developed to evaluate c_f from measured velocity profiles; the best known of these is that of Clauser.[5] This technique correlates the measured profiles with a set of theoretical profiles derived from the law of the wall as

$$U/U_1 = (U_\tau/U_1)\{A \log[(yU_1/\nu)(U_\tau/U_1)] + B\} \tag{23}$$

where

$$U_\tau/U_1 = [(\rho_1/\rho_0)(c_f/2)]^{1/2} \tag{24}$$

The use of this technique, however, encounters difficulties in the present case, since the appropriate value of the constant B is not known. As mentioned previously, B is a function of surface roughness; but for practical aircraft surfaces, which contain a variety of roughness elements, this function has not been determined yet.

Therefore, an alternate technique has been used here to evaluate c_f, which is similar in principle to Clauser's method, but it uses only the slope of the profiles as a basis of correlation and does not require the knowledge of B. The essence of this method is as follows: Eq. (23) can be written in the form

$$U/U_1 = (U_\tau/U_1)A \log y + \text{const} \tag{25}$$

Thus, by plotting the velocity profile in a semilogarithmic diagram, U/U_1 vs $\log y$, one can determine the quantity U_τ/U_1 from the slope of the line passing through the experimental points; that is,

$$U_\tau/U_1 = (1/A)d(U/U_1)/d(\log y)] \tag{26}$$

The local skin-friction coefficient can then be calculated from

$$c_f = 2(\rho_0/\rho_1)(U_\tau/U_1)^2 \tag{27}$$

This technique of determing c_f is demonstrated in Fig. 12 for the test station C-3. The experimental data fall along a straight line except in the outer region where the law of the wall is not valid. The appropriate value of U_τ/U_1 is determined by comparing the experimental profile with a set of radial lines and selecting that member of the set that has the same slope as the experimental profile. In the case presented, both profiles appear to have the same slope; that is, no appreciable change can be detected in the local skin-friction coefficient as a result of pressurization. Similar results are found at most of the test stations (Table 2). There are two exceptions, however; stations A-1 and B-3, where c_f is higher in the unpressurized condition. But this is understandable, since in these cases δ^* and θ are considerably smaller in the unpressurized condition, and, according to the $c_f = f(R_\theta)$ relation, c_f would necessarily be greater. The variation of c_f within the same test section is related to the local pressure gradient: an adverse gradient results in a lower skin friction, and a favorable gradient results in a higher skin friction. This also explains why the c_f values are higher at section C than at section A, although one would expect the contrary because of the decreasing trend of c_f with increasing Reynolds number.

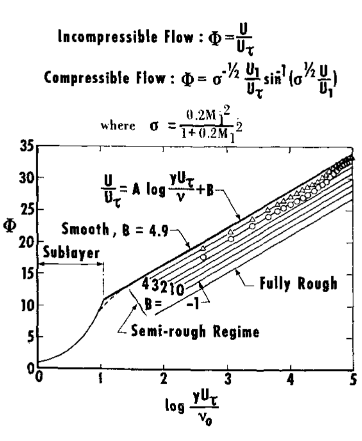

Fig. 13 Boundary-layer profiles presented in terms of the law of the wall.

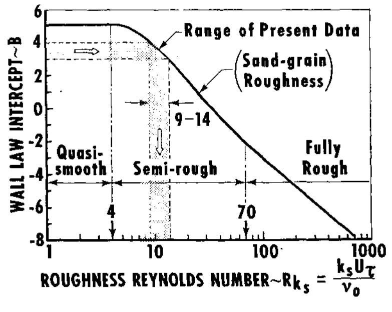

Fig. 14 Estimation of equivalent sand-grain roughness.

Table 2 Local skin-friction coefficients as evaluated by the wall law slope method

Test station	A-1	A-2[a]	A-4	B-1	B-2	B-3	C-1	C-2	C-3	C-4
Pressurized	0.00160	0.00135	0.00155	0.00160	0.00155	0.0016	0.00175	0.00175	0.00165	0.00190
Unpressurized	0.00175	0.00135	0.00155	0.00160	0.00155	0.0017	0.00175	0.00175	0.00165	0.00190

[a] No data are given for station A-3, since the distorted profiles recorded there are not suitable for evaluation of c_f.

The accuracy of the method by which c_f is determined greatly depends on the precision with which the slope of the experimental profile is evaluated. The experiental scatter makes this task difficult and introduces some degree of uncertainty, so that the accuracy is probably not better than ±3%. The results can be verified, however, by replotting the profiles in terms of the law of the wall $U/U_\tau = f(yU_\tau/\nu)$. Good correlation can be expected between the experimental profile and the law of the wall only if the correct value of U_τ, i.e., c_f is used in the normalizing process. An example is shown in Fig. 13, which demonstrates the correlation of two typical profiles with the law of the wall. The heavy line represents the theoretical profile for a smooth surface, and the parallel lines below correspond to increasing surface roughness. The experimental profiles presented show good correlation with the law of the wall but lie clearly below the "smooth" line. These profiles, and all of the others, indicate that the applicable values of B are within the range of $B = 3$ to 4.

Based on this result, the equivalent sand-grain roughness of the fuselage surface can be estimated. Equivalent sand-grain roughness k_s is defined as that size of sand grains, distributed on the surface with minimum spacing, which would produce the same skin friction as the original surface with an arbitrary roughness. Nikuradse[6] has determined the relation between the wall law constant B and the roughness Reynolds Number $R_{ks} = k_sU_\tau/\nu_0$ for pipes with various sand-grain roughness (Fig. 14). From this relation we may conclude that the range of $B = 3$ to 4, characteristic to the fuselage surface, has a corresponding range of $R_{k_s} = 14$ to 9. Thus, we find that the sand-grain size equivalent to the fuselage surface roughness is approximately

$$k_s = 0.0014 \text{ to } 0.0022 \text{ in.}$$

Although this figure seems very small, it is several times greater than the admissible roughness height, i.e., the maximum size of roughness elements that still do not increase the skin friction. This limit is set as $R_{k_{\text{adm}}} = 4$, which corresponds to approximately

$$k_{\text{adm}} = 0.00056 \text{ in.}$$

Data on roughness characteristics of practical aircraft surfaces are very scarce; thus, the preceding figures may be of some value for roughness drag estimation purposes.

Conclusions

The analysis of the boundary-layer characteristics measured at several points of a Boeing 720 fuselage in both pressurized and unpressurized conditions leads to the following conclusions:

1) The effect of pressurization is manifested in an increased boundary-layer momentum thickness around the fuselage.

2) The increment in θ stems not only from skin bulging, but also from such effects as leakage of the pressurized air and outflows associated with the pressurization system.

3) No quantitative breakdown could be made as to the relative magnitude of these effects; it is contemplated, however, that the leakage and air exhaustion are even more important factors than the skin bulging.

4) The amount of leakage is different for each individual airplane. Thus, the numerical results of the present experiment are valid only for the particular airplane tested. However, if we regard the information presented on an order-of-magnitude basis, the results probably can be generalized.

5) The pressurization increases the drag of the fuselage by approximately 5%. This corresponds to an increment of $1\frac{1}{4}\%$ in the total airplane drag in cruising condition where the drag contribution of the fuselage is approximately 25%.

6) The effects of skin bulging on today's subsonic airliners appear to be insignificant. This, however, may not be the case in the near future when airliners reach supersonic speeds. The small skin bulges may then produce local shock waves and thus may cause a more severe drag increment.

References

[1] Schlichting, H., *Boundary Layer Theory* (McGraw-Hill Book Co., Inc., New York, 1960), 4th ed.

[2] Vincenti, W. G., "Non-equilibrium flow over a wavy wall," J. Fluid Mech. 6, 481–496 (1959).

[3] Young, A. D., "The calculation of the total and skin friction drags of bodies of revolution at zero incidence," Aeornautical Research Council R&M 1874 (1939).

[4] Squire, H. B. and Young, A. D., "The calculation of profile drag of airfoils," Areonautical Research Council R&M 1838 (1937).

[5] Clauser, F. H., "Turbulent boundary layers in adverse pressure gradients," J. Aeronaut. Sci. **21**, 91–108 (1954).

[6] Nikuradse, J., "Laws of flow in rough pipes," NACA Tech. Memo 1292 (1950).